Theoretical and Applied Mechanics Letters 11 (2021) 100279

Contents lists available at ScienceDirect

Theoretical and Applied Mechanics Letters

journal homepage: www.elsevier.com/locate/taml

Letter

On the capability of the curvilinear immersed boundary method in predicting near-wall turbulence of turbulent channel flows

Fei Liao[a,b], Xiaolei Yang[a,c,*]

[a] State Key Laboratory of Nonlinear Mechanics, Institute of Mechanics, Chinese Academy of Sciences, Beijing 100190, China
[b] School of Aeronautics, Northwestern Polytechnical University, Xi'an 710072, China
[c] School of Engineering Sciences, University of Chinese Academy of Sciences, Beijing 100049, China

ARTICLE INFO

Article history:
Received 27 May 2021
Revised 20 June 2021
Accepted 20 June 2021
Available online 28 July 2021

Key words:
Immersed boundary method
Turbulent channel flow
Wavenumber-frequency spectra
Near-wall turbulence

ABSTRACT

The immersed boundary method has been widely used for simulating flows over complex geometries. However, its accuracy in predicting the statistics of near-wall turbulence has not been fully tested. In this work, we evaluate the capability of the curvilinear immersed boundary (CURVIB) method in predicting near-wall velocity and pressure fluctuations in turbulent channel flows. Simulation results show that quantities including the time-averaged streamwise velocity, the rms (root-mean-square) of velocity fluctuations, the rms of vorticity fluctuations, the shear stresses, and the correlation coefficients of u' and v' computed from the CURVIB simulations are in good agreement with those from the body-fitted simulations. More importantly, it is found that the time-averaged pressure, the rms and wavenumber-frequency spectra of pressure fluctuations computed using the CURVIB method agree well with the body-fitted results.

Turbulent flows in real-world applications often happen with complex geometry. The immersed boundary (IB) method, which is based on non-body-fitted grids, does not require complicated grid generation process, providing an efficient approach for simulating flows with complex boundaries. Although the immersed boundary method has been applied to different flow problems [1-4], its capability in simulating near-wall turbulence has not been systematically evaluated, which is of vital importance for some applications, e.g., the noise prediction [5, 6]. The fractional step method is often employed for solving the incompressible flows [7-9]. When the immersed boundary method is employed with the fractional step method, the velocity reconstruction is often applied at the intermediate velocity instead of the final velocity after the projection step. This causes an inconsistency between the reconstructed velocity boundary condition and the divergence free condition. To address this problem, Kim et al. [10] introduced a source/sink term to the continuity equation for cells containing the immersed boundary. Ikeno and Kajishima [11] proposed a consistent scheme and examined the capability of the proposed scheme in predicting the mean velocity and velocity fluctuations for incompressible flows in aligned channel, inclined channel, circular pipe and nuclear rod-bundle. In the work by Kang et al. [12], the reconstructed velocity is corrected using the least square method to satisfy the constraint of global mass conservation. The capability of the proposed approach was then assessed for predicting the mean streamwise velocity, rms (root-mean-square) of velocity fluctuations and wall-pressure power spectra in turbulent channel flows. In this work, the curvilinear immersed boundary (CURVIB) method [8, 13] is employed, which adopts a curvilinear grid as the background grid and allows approximately distributing grid nodes in a way following the immersed boundaries whenever it is possible. In the CURVIB approach, a correction term, which is often very small, is uniformly applied to the reconstructed velocity to ensure the global mass conservation. The objective of this work is to systematically examine the CURVIB method in predicting near-wall velocity and pressure fluctuations of the turbulent channel flow at $Re_\tau = u_\tau \delta/\nu = 180$, where u_τ is the friction velocity, δ is the half height of the channel and ν is the kinematic viscosity.

The virtual flow simulator (VFS) [14] is employed in this work for direct numerical simulation (DNS) of the fully developed turbulent channel flow. The governing equations are the three-dimensional unsteady incompressible Navier-Stokes equations in

* Corresponding author.
E-mail address: xyang@imech.ac.cn (X. Yang).

https://doi.org/10.1016/j.taml.2021.100279

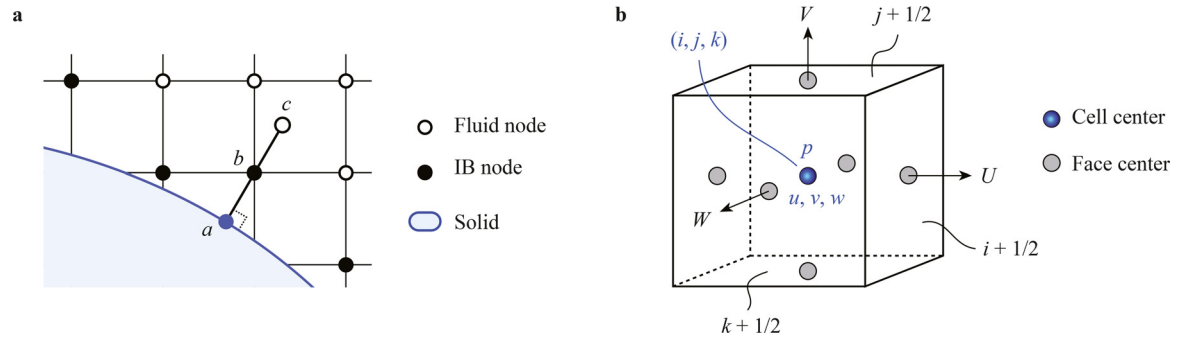

Fig. 1. A schematic for **a** the reconstruction of the velocity at IB node and **b** the storage arrangement of velocity, pressure and contravariant velocity.

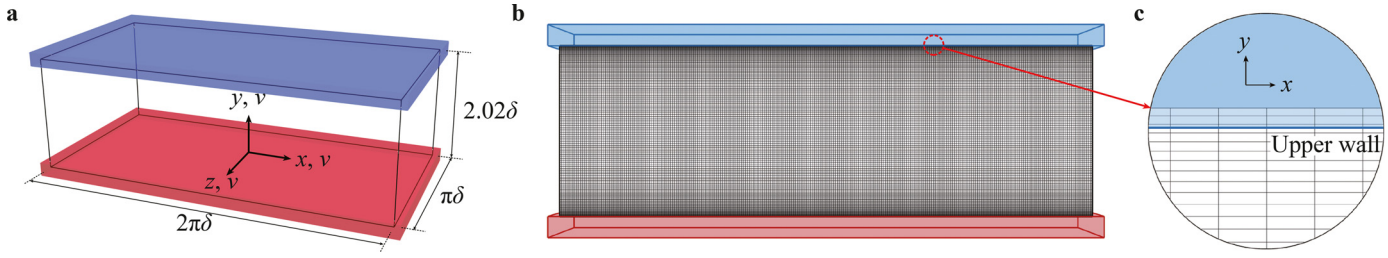

Fig. 2. A schematic for the setup of the immersed boundary simulation with **a** coordinate definition, **b** grid distribution and **c** grid nodes near the upper wall. Note that the grid for the immersed boundary simulation is designed in a way that the top and bottom walls do not coincide with grid nodes in the wall-normal direction.

curvilinear coordinates shown as follows:

$$J\frac{\partial U^j}{\partial \xi^j} = 0,$$
$$\frac{1}{J}\frac{\partial U^i}{\partial t} = \frac{\xi_l^i}{J}\left[-\frac{\partial}{\partial \xi^j}\left(U^j u_l\right) - \frac{1}{\rho}\frac{\partial}{\partial \xi^j}\left(\frac{\xi_l^j p}{J}\right) + \frac{\mu}{\rho}\frac{\partial}{\partial \xi^j}\left(\frac{g^{jk}}{J}\frac{\partial u_l}{\partial \xi^k}\right)\right], \tag{1}$$

where x_i and ξ^i are the Cartesian and curvilinear coordinates, respectively, $\xi_l^i = \partial \xi^i / \partial x_l$ are the transformation metrics, J is the Jacobian of the geometric transformation, u_i is the i-th component of the velocity vector in Cartesian coordinates, $U^i = (\xi_m^i / J) u_m$ is the contravariant volume flux, $g^{jk} = \xi_l^j \xi_l^k$ are the components of the contravariant metric tensor, ρ is the density, μ is the dynamic viscosity, and p is the pressure. The governing equations are discretized in space using a second-order accurate central differencing scheme, and integrated in time using the fractional step method. An algebraic multigrid acceleration along with generalized minimal residual method (GMRES) solver is used to solve the pressure Poisson equation. A matrix-free Newton-Krylov method is used for solving the discretized momentum equation. More details about the flow solver can be found in Refs. [14-16].

In the CURVIB method, the background grid nodes are classified as solid nodes inside solid body and fluid nodes in the fluid. The fluid node with at least one neighbour of solid nodes is marked as the IB node (e.g. point b in Fig. 1a). The velocity of the IB node is reconstructed using the velocity at point c and the velocity at the boundary to supply boundary conditions for the outer flow simulations, in which the velocity at c is interpolated from the surrounding fluid nodes. For DNS and wall-resolved large-eddy simulation, the linear interpolation is employed for the velocity reconstruction. For flows at high Reynolds number, computationally efficient wall-modeled large-eddy simulation is preferred, in which the velocity is reconstructed using a wall model [17-22]. The CURVIB method employs a hybrid staggered/non-staggered grid layout, as shown in Fig. 1b, for solving satisfying the divergence-free conditions. The equations are advanced in time using a second-order fractional step method. The procedure for advancing the flow field for one time step is summarized as follows:

1 Solve the momentum equation for the intermediate velocity at volume centers, with the velocity reconstructed at the IB nodes serving as boundary conditions;
2 Compute the contravariant velocity at the face centers using the velocities at volume centers;
3 Correct the contravariant velocity at face centers, which are next to IB nodes, to satisfy the global mass conservation;
4 Solve the Poisson equation with its right-hand-side term computed using the contravariant velocities;
5 Obtain the final velocity and pressure for this time step.

More details about the CURVIB method can be found in Refs. [8, 9, 23, 24].

We carry out simulations of fully developed turbulent channel flow to evaluate the capability of the CURVIB method in predicting the near-wall turbulence. The Reynolds number based on the wall friction velocity is $Re_\tau = u_\tau \delta / \nu = 180$, where ν is the kinematic viscosity, $u_\tau = (\tau_w / \rho)^{\frac{1}{2}}$ is the wall friction velocity, and δ is the half height of the channel. The flow is driven by a mean pressure gradient in the streamwise direction to maintain a constant mass flux.

A schematic for the setup of the immersed boundary simulation is shown in Fig. 2. The streamwise, wall-normal and spanwise directions are denoted by x, y and z, respectively. The size of the computational domain is $L_x \times L_y \times L_z = 2\pi\delta \times 2.02\delta \times \pi\delta$, in which the computational domain in wall-normal direction is set in the range of $y \in [-0.01, 2.01]$ with two manually located walls at $y = 0$ and $y = 2$ between grid nodes. The numbers of grid nodes are $N_x \times N_y \times N_z = 256 \times 134 \times 256$. In order to fully examine the accuracy, the grid for the immersed boundary simulation is designed in a way that the top and bottom walls do not coincide with grid nodes in wall-normal direction. The wall-normal grid spacing near the upper and lower walls is $\Delta y = 0.0044\delta$, with the corresponding $\Delta y^+ = \Delta y u_\tau / \nu = 0.80$. The grid nodes are uniformly distributed in the streamwise and spanwise directions, respectively, with the grid spacings calculated to be $\Delta x^+ = 4.4$

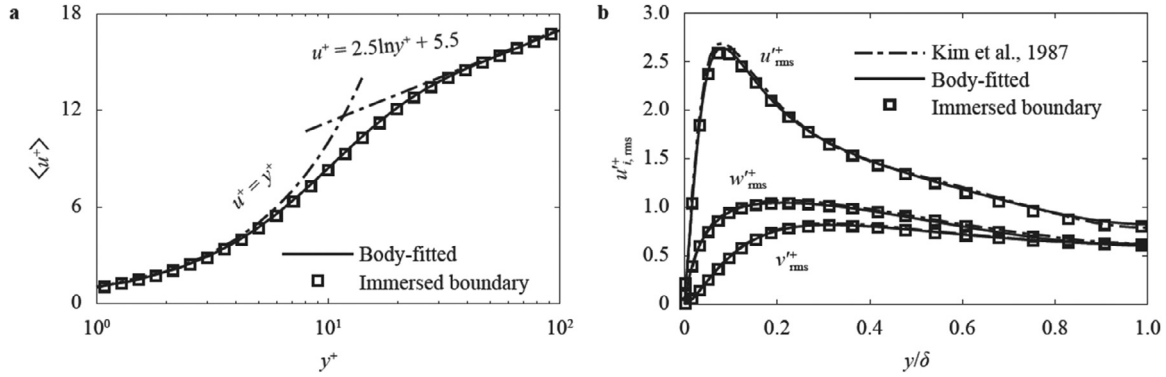

Fig. 3. Comparison of **a** time-averaged streamwise velocity and **b** root-mean-square of velocity fluctuations.

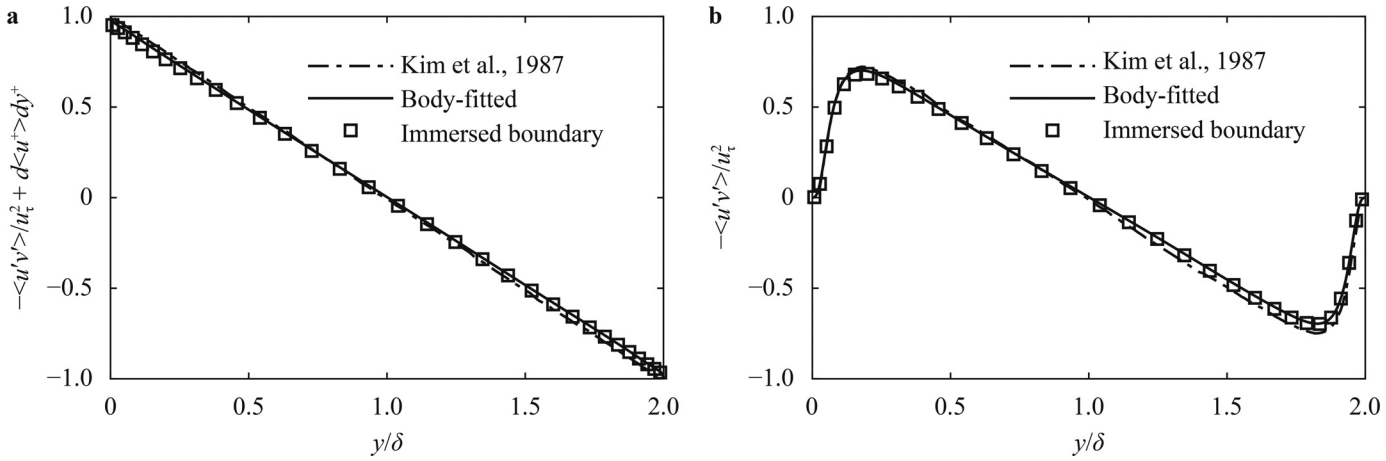

Fig. 4. Comparison of **a** total shear stress $-\langle u'v' \rangle/u_\tau^2 + \mathrm{d}\langle u^+ \rangle/\mathrm{d}y^+$ and **b** Reynolds shear stresses $-\langle u'v' \rangle/u_\tau^2$.

and $\Delta z^+ = 2.2$, respectively. Periodic boundary conditions are applied in the streamwise and spanwise directions. The time step is set to $\Delta t = 0.004\pi\delta/u_\mathrm{b}$, which corresponds to a CFL (Courant–Friedrichs–Lewy) number of $u_b \Delta t/\Delta x = 0.5$, where u_b is the bulk velocity. This setup for time step indicates about 500 steps for one flow through. For the body-fitted simulation, the size of the computational domain is $L_x \times L_y \times L_z = 2\pi\delta \times 2\delta \times \pi\delta$ with the number of grid nodes of $N_x \times N_y \times N_z = 256 \times 128 \times 256$. The height of the first off-wall grid node is $\Delta y = 0.004\delta$, with the corresponding $\Delta y^+ = 0.72$. The time step for the body-fitted simulation is set to be the same with that of the immersed boundary simulation. Both simulations are firstly carried out until the flows are fully developed, then additional simulations are carried out to obtain turbulence statistics for about 100 flow throughs.

We first compare the profiles of mean streamwise velocity in Fig. 3a and the root-mean-square of the velocity fluctuations in Fig. 3b from the immersed boundary simulation with those from the body-fitted simulation carried out by Kim et al. [25]. As seen, the immersed boundary predictions agree well with the body-fitted results and the reference. Then, we compare the profiles of total shear stress and Reynolds shear stress in Fig. 4. As discussed in Ref. [26], the following equation leads to the profile of a straight line in Fig. 4a for the total shear stress:

$$\nu \frac{\mathrm{d}\langle u \rangle}{\mathrm{d}y} - \langle u'v' \rangle = \frac{\tau_w}{\rho}\left(1 - \frac{y}{\delta}\right) \Rightarrow \frac{\mathrm{d}\langle u^+ \rangle}{\mathrm{d}y^+} - \frac{\langle u'v' \rangle}{u_\tau^2} = 1 - \frac{y}{\delta}. \quad (2)$$

Meanwhile, in the middle of the channel at $y/\delta = 1$, due to $\mathrm{d}\langle u^+ \rangle/\mathrm{d}y^+ = 0$, the Reynolds shear stress $-\langle u'v' \rangle/u_\tau^2$ should have a slope of -1 with respect to y/δ, as shown in Fig. 4b. It is observed clearly that both total shear stress and Reynolds stress from the immersed boundary simulations agree well with body-fitted simulation and the reference. We further compare the correlation coefficients of u' and v' in Fig. 5. It can be seen that there is a relatively strong correlation between u' and v' in a wide range of y/δ near the wall, which indicates certain coherent motions in the wall region. As discussed in Ref. [25], an observed weak peak at $y^+ \approx 12$ shows the location of the maximum production and the maximum streamwise velocity fluctuation. It is observed that all these features are well predicted by the immersed boundary simulations.

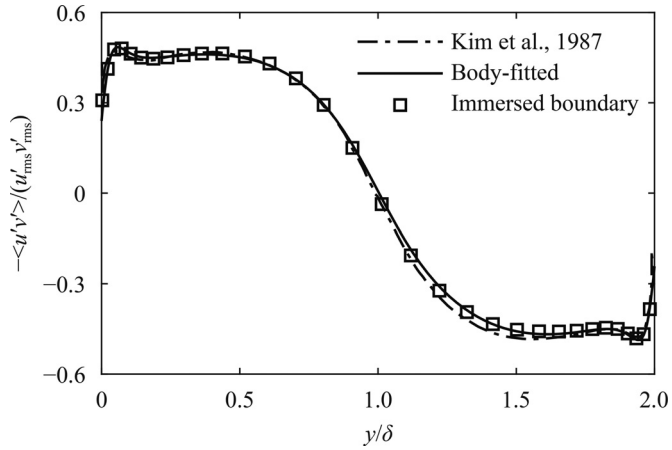

Fig. 5. Correlation coefficients of u' and v'.

Next, we compare the profiles of rms of the vorticity fluctuations in Fig. 6. It can be seen the immersed boundary simulation

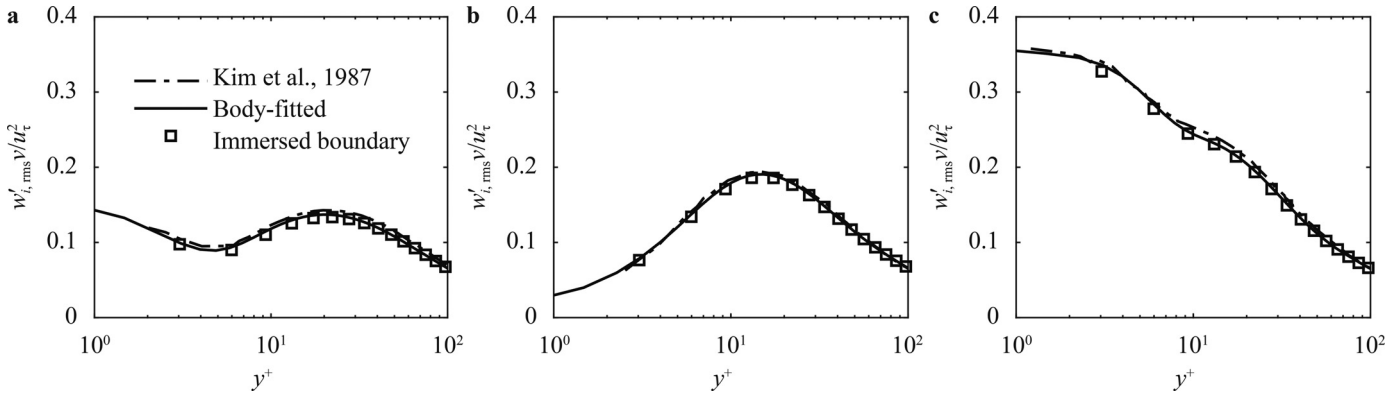

Fig. 6. Root-mean-square of vorticity fluctuations **a** $\omega'_{x,\mathrm{rms}}$, **b** $\omega'_{y,\mathrm{rms}}$ and **c** $\omega'_{z,\mathrm{rms}}$, normalized by mean shear.

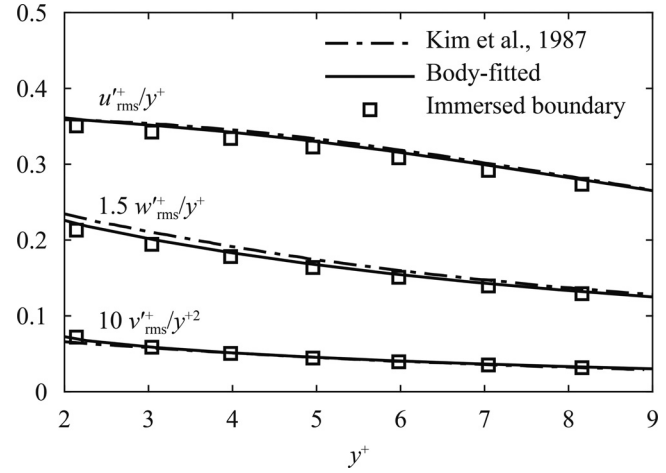

Fig. 7. Comparison of the near-wall behavior of velocity fluctuations: u'^+_{rms}/y^+, $v'^+_{\mathrm{rms}}/y^{+2}$ and w'^+_{rms}/y^+.

can accurately predict the vorticity fluctuations. As is explained in Ref. [25], the local minimum and the local maximum of the streamwise vorticity indicate the edge and centre of the vortex, respectively, leading to an estimation of the centre of the streamwise vortex located at $y^+ = 20$ with radius $r^+ = 15$.

Then, we examine the near-wall scaling of velocity fluctuations $u'_{i,\mathrm{rms}}$ in Fig. 7 to evaluate the capability of the employed CURVIB method in predicting the near-wall behavior, where the boundary conditions are not directly applied at the wall. Applying the no-slip boundary condition and continuity equation to the Taylor series expansion of the velocity components [26], it can be obtained that the streamwise u'^+_{rms} and spanwise w'^+_{rms} have a linear scaling of y^+, while the wall-normal v'^+_{rms} has a behavior of y^{+2} scaling, as shown in Fig. 7. It is observed that the immersed boundary method can accurately predict such scalings.

At last, we focus on the capability of the immersed boundary method in predicting time-averaged pressure and statistics of pressure fluctuations. We show the profiles of time-averaged pressure and rms of pressure fluctuations in Fig. 8. It is observed that the predictions of the immersed boundary simulation agree well with those from the body-fitted simulations, although somewhat differences are observed for the peak of the time-averaged pressure. In Fig. 9, we compare the normalized wavenumber-frequency spectra of the pressure fluctuations at two wall-normal locations, which are compted using the following equations:

$$\chi(y;k_x,\omega) = \frac{|p\prime(y;k_x,\omega)|^2}{\Sigma_{i=-N_x/2}^{N_x/2-1}\Sigma_{j=-N_t/2}^{N_t/2-1}\left|p\prime\left(y;k_{x,i},\omega_j\right)\right|^2}, \tag{3}$$

where k_x and ω are the streamwise wavenumber and frequency, respectively, and $p\prime(y;k_x,\omega)$ is the spatial-temporal discrete Fourier transform (DFT) of pressure fluctuation $p\prime(y;x,t) = p(y;x,t) - \langle p(y;x,t)\rangle$. Ensemble averaging for $|p\prime(y;k_x,\omega)|^2$ is carried out in the spanwise direction and in time with 50% overlapping. To make comparisons between the two simulations, the body-fitted result is shown by contour floods, whereas the immersed boundary result is indicated by red solid contour lines. It

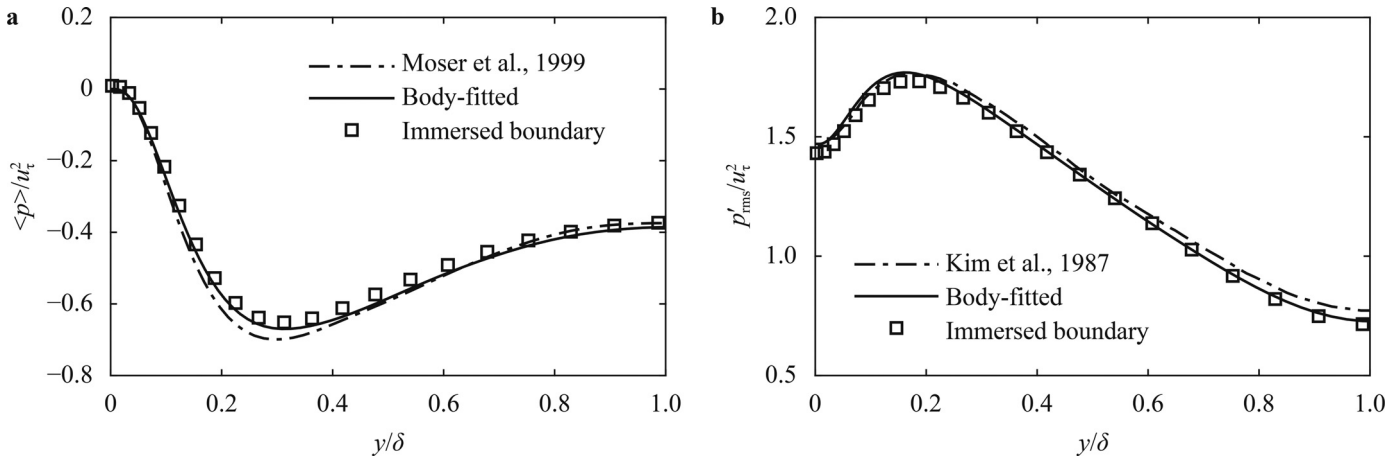

Fig. 8. Comparison of **a** time-averaged pressure and **b** root-mean-square of the pressure fluctuations.

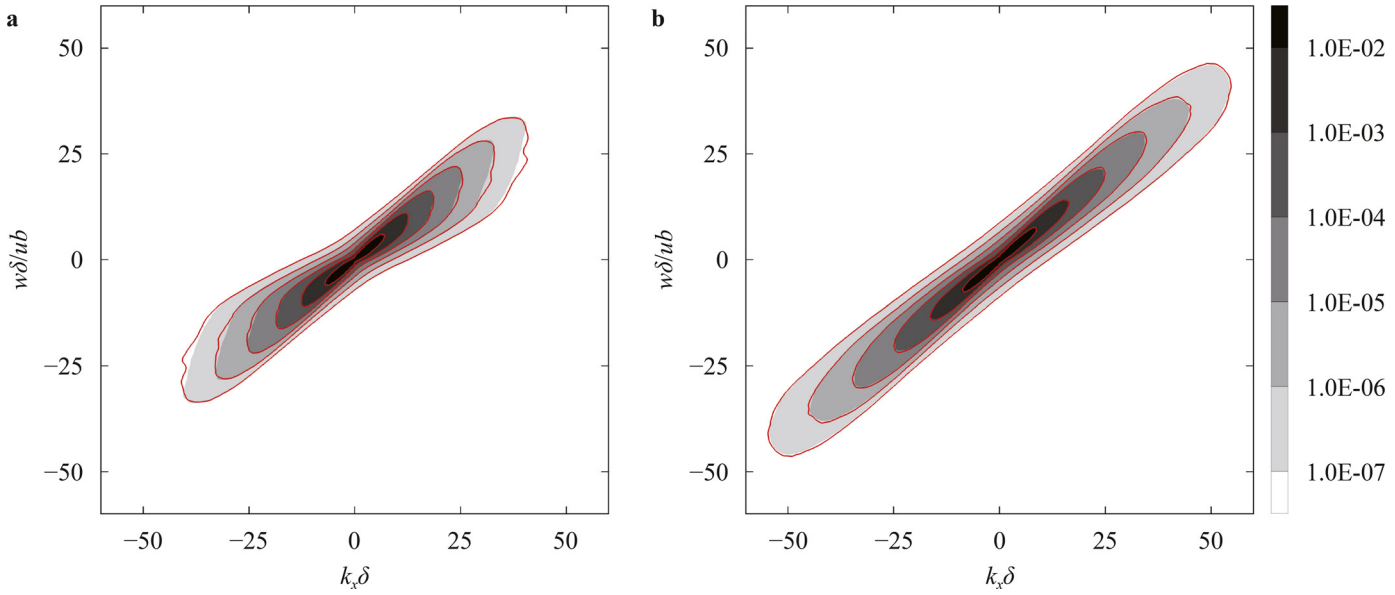

Fig. 9. Normalized wavenumber-frequency spectra of pressure fluctuations at **a** wall and **b** $y^+ = 30$ computed from the two simulations. To make comparisons, the body-fitted result is shown by contour floods, whereas the immersed boundary result is indicated by red solid contour lines.

is observed that the energy-containing regions of pressure fluctuations predicted by the two simulations are almost identical at the considered wall-normal locations with slight differences observed at high wavenumber and frequency for the spectra at the wall, which indicates that the immersed boundary method is able to predict the space-time structure of pressure fluctuations at the same accuracy as the body-fitted method.

In this work, we examine the capability of the curvilinear immersed boundary method in predicting near-wall turbulence of the turbulent channel flow at Reynolds number $Re_\tau = 180$ by comparing its predictions with those from the simulation of a body-fitted method. Quantities including mean and fluctuations of velocity, vorticity and pressure, shear stresss, correlation coefficient of $u\prime$ and $v\prime$, near-wall scaling of velocity fluctuations and wavenumber-frequency spectra of pressure fluctuations are compared. Two conclusions can be drawn as follows: (1) The accuracy of the curvilinear immersed boundary method in predicting statistics of velocity and pressure fluctuations is almost the same as that of the body-fitted method; (2) For the wavenumber-frequency spectra of pressure fluctuations, minor fluctuations are observed at high wavenumber and high frequency for the immersed boundary predictions, which might not be of great significance as the energy at that wave number and frequency is several orders of magnitude smaller than the maximum value.

Since the Cartesian grid is employed in this work, similar conclusions are expected for the immersed boundary method based on the Cartesian grid with similar near wall treatments. Only the case of the turbulent channel flow at a low Reynolds number is tested in this work for which DNS is feasible. Further studies need to be carried out using cases at high Reynolds numbers to test LES and the immersed boundary method with wall models. Furthermore, evaluation on the near wall accuracy of the CURVIB method will be carried out in the future work for cases with complex boundaries.

Declaration of Competing Interest

The authors declare that there are no known competing financial interests or personal relationships that could have appeared to influence the work reported in this paper.

Acknowledgment

This work was supported by the National Natural Science Foundation of China (NSFC) Basic Science Center Program for “Multi-scale Problems in Nonlinear Mechanics” (No. 11988102) and the Strategic Priority Research Program, Chinese Academy of Sciences (CAS) (No. XDB22040104).

References

[1] R. Mittal, G. Iaccarino, Immersed boundary methods, Annu. Rev. Fluid Mech. 37 (2005) 239–261.
[2] F. Sotiropoulos, X.L. Yang, Immersed boundary methods for simulating fluid–structure interaction, Prog. Aerosp. Sci. 65 (2014) 1–21.
[3] W.-X. Huang, F.-B. Tian, Recent trends and progress in the immersed boundary method, P. I. Mech. Eng. C-J. Mec. 233 (2019) 7617–7636.
[4] B.E Griffith, N.A. Patankar, Immersed methods for fluid–structure interaction, Annu. Rev. Fluid Mech. 52 (2020) 421–448.
[5] R. Li, B. Yang, Z.X. Yang, et al., Error of large-eddy simulation in the wall pressure fluctuation of a turbulent channel flow, Theor. App. Mech. Lett. 11 (2021) 100248.
[6] Z.T. Zhou, S.Z. Wang, Far-field approximations to the derivatives and integrals of the green's function for the ffocws williams and hawkings equation, arXiv preprint arXiv: 2105.05042, 2021.
[7] H. Le, P. Moin, An improvement of fractional step methods for the incompressible navier-stokes equations, J. Comput. Phys. 92 (1991) 369–379.
[8] L. Ge, F. Sotiropoulos, A numerical method for solving the 3D unsteady incompressible Navier–Stokes equations in curvilinear domains with complex immersed boundaries, J. Comput. Phys. 225 (2007) 1782–1809.
[9] I. Borazjani, L. Ge, F. Sotiropoulos, Curvilinear immersed boundary method for simulating fluid structure interaction with complex 3d rigid bodies, J. Comput. Phys. 227 (2008) 7587–7620.
[10] J. Kim, D. Kim, H. Choi, An immersed-boundary finite-volume method for simulations of flow in complex geometries, J. Comput. Phys. 171 (2001) 132–150.
[11] T. Ikeno, T. Kajishima, Finite-difference immersed boundary method consistent with wall conditions for incompressible turbulent flow simulations, J. Comput. Phys. 226 (2007) 1485–1508.
[12] S. Kang, G. Iaccarino, F. Ham, et al., Prediction of wall-pressure fluctuation in turbulent flows with an immersed boundary method, J. Comput. Phys. 228 (2009) 6753–6772.
[13] A. Gilmanov, F. Sotiropoulos, A hybrid cartesian/immersed boundary method for simulating flows with 3d, geometrically complex, moving bodies, J. Comput. Phys. 207 (2005) 457–492.
[14] X.L. Yang, F. Sotiropoulos, R.J Conzemius, et al., Large-eddy simulation of turbulent flow past wind turbines/farms: the Virtual Wind Simulator (VWiS), Wind Energy 18 (2015) 2025–2045.
[15] S. Kang, A. Lightbody, C. Hill, et al., High-resolution numerical simulation of turbulence in natural waterways, Advan. Water Resour. 34 (2011) 98–113.
[16] X.L. Yang, F. Sotiropoulos, A new class of actuator surface models for wind turbines, Wind Energy 21 (2018) 285–302.

[17] F. Roman, V. Armenio, J. Fröhlich, A simple wall-layer model for large eddy simulation with immersed boundary method, Phys. Fluids 21 (2009) 101701.
[18] X.I.A. Yang, J. Sadique, R. Mittal, et al., Integral wall model for large eddy simulations of wall-bounded turbulent flows, Phys. Fluids 27 (2015) 025112.
[19] S.Z. Wang, B.J. Shi, Y.H. Li, et al., A large eddy simulation of flows around an underwater vehicle model using an immersed boundary method, Theor. App. Mech. Lett. 6 (2016) 302–305.
[20] M. Ma, W.-X. Huang, C.-X. Xu, A dynamic wall model for large eddy simulation of turbulent flow over complex/moving boundaries based on the immersed boundary method, Phys. Fluids 31 (2019) 115101.
[21] F. Liao, X.L. Yang, S.Z. Wang, et al., Grid-dependence study for simulating propeller crashback using large-eddy simulation with immersed boundary method, Ocean Eng. 218 (2020) 108211.
[22] M. Ma, W.-X. Huang, C.-X. Xu, et al., A hybrid immersed boundary/wall-model approach for large-eddy simulation of high-reynolds-number turbulent flows, Int. J. Heat Fluid Fl. 88 (2021) 108769.
[23] A. Khosronejad, S. Kang, I. Borazjani, et al., Curvilinear immersed boundary method for simulating coupled flow and bed morphodynamic interactions due to sediment transport phenomena, Advan. Water Resour. (2011).
[24] S.L. Li, X.L. Yang, G.D. Jin, et al., Wall-resolved large-eddy simulation of turbulent channel flows with rough walls, Theor. App. Mech. Lett. 11 (2021) 100228.
[25] J. Kim, P. Moin, R. Moser, Turbulence statistics in fully developed channel flow at low Reynolds number, J. Fluid Mech. 177 (1987) 133–166.
[26] S.B. Pope, Turbulent Flows, IOP Publishing, 2001.